Multilevel 2D Bar Codes: Towards High Capacity Storage Modules for Multimedia Security and Management

Renato Villán, Sviatoslav Voloshynovskiy, Oleksiy Koval, and Thierry Pun

Computer Vision and Multimedia Laboratory, Dept. of Computer Science,
University of Geneva, 24 rue Général-Dufour, 1211 Geneva 4, Switzerland

ABSTRACT

In this paper, we deal with the design of high-rate multilevel two-dimensional (2D) bar codes for the print-and-scan channel. Firstly, we derive an upper bound on the maximum achievable rate of these codes by studying an inter-symbol interference (ISI) free, perfectly synchronized, and noiseless print-and-scan channel, in which the printer device uses halftoning to simulate multiple gray levels. Secondly, we briefly review three state-of-the-art coded modulation techniques for the additive white Gaussian noise channel (AWGN) in the high signal-to-noise (SNR) ratio regime, namely, multilevel coding with multistage decoding (MLC/MSD), multilevel coding with parallel independent decoding (MLC/PID), and bit-interleaved coded modulation (BICM). Thirdly, we present a new model of the print-and-scan channel specifically adapted to the multilevel 2D bar code application. This model, inspired by our experimental work, assumes no ISI and perfect synchronization, but independence between the channel input and the noise is not supposed. We study the problem of finding the information capacity of our channel model and extend the theory of MLC/MSD to this type of channels. Finally, we present experimental results confirming the validity of our channel model, and showing that multilevel 2D bar codes using MLC/MSD can reliably achieve the high-rate storage requirements of many multimedia security and data management applications.

Keywords: 2D bar codes, high capacity storage, print-and-scan channel, multilevel coded modulation.

1. INTRODUCTION

Two-dimensional bar codes are very attractive for various applications, where a significant amount of data needs to be stored onto paper, plastic or other information carriers. Another attractive characteristic of 2D bar codes as information storage modules consists in their low price: cheap printer and reader devices exist for the most common media. For example, laser or inkjet halftone printers can be used for printing on paper; laser engraving, a cheap and high quality technique, can be used for printing on plastic; furthermore, cheap and low-resolution charged coupled device (CCD) based scanners or digital cameras, like those present in cell phones, can be used for reading the printed information.

For the above reasons, 2D bar codes are being considered for new emerging applications such as *M-ticketing*, where they carry selected information of a ticket that is received via a mobile phone; *reliable and secure personal identification*,[1] where they store personal biometric data on the identification document; and *visual communications with side information*,[2] where they can be used as an auxiliary channel conveying additional data for improving visual communications.

However, current 2D bar codes do not offer enough storage capability for these new applications. In part, this is because most of them use only black and white (B&W) 2D symbols for representing data and corresponding binary coding technology. Only few proposals exist (commercial and non-commercial) that use multiple gray levels or colors for the 2D symbols. We call this type of symbologies *multilevel 2D bar codes*. Although multilevel 2D bar codes can potentially increase the achievable rates, in bytes per square inch (bytes/in^2), of B&W symbologies, little research has been done on how to efficiently design and implement this approach. Therefore, the main goal of this paper is to give a number of guidelines for the design of cheap and high-rate multilevel 2D bar codes.

For further information contact S. Voloshynovskiy. E-mail: svolos@cui.unige.ch (http://sip.unige.ch)

This paper is organized as follows. The description of the problem framework and a review of multilevel coding for the AWGN channel is given in Section 2. A new model for the print-and-scan channel adapted to the multilevel 2D bar code application is presented in Section 3. The extension of the theory of multilevel coding to this new channel model is considered in Section 4. Computer simulation results are presented in Section 5. Finally, Section 6 concludes the paper and describes future work.

Notations. We use capital letters X to denote scalar random variables, bold capital letters $\mathbf{X}$ to denote vector random variables and corresponding small letters x and $\mathbf{x}$ to denote the realizations of scalar and vector random variables, respectively. The probability mass (resp. density) function or p.m.f. (resp. p.d.f.) of a discrete (resp. continuous) random variable X is denoted $p_X(\cdot)$ (resp. $f_X(\cdot)$). When no confusion is possible we write $p(x)$ (resp. $f(x)$) instead of $p_X(x)$ (resp. $f_X(x)$). We use $X \sim p_X(\cdot)$ to indicate that the random variable X is distributed according to $p_X(\cdot)$. The mathematical expectation of a random variable $X \sim p_X(\cdot)$ is denoted by $\mathrm{E}_{p_X}[X]$ or simply by $\mathrm{E}[X]$ or μ_X. $\mathrm{Var}[X]$ or σ_X^2 denote the variance of X. Calligraphic letters $\mathcal{X}$ denote sets and $|\mathcal{X}|$ denotes the cardinality of $\mathcal{X}$. The entropy (resp. differential entropy) of a discrete (resp. continuous) random variable X is denoted $\mathrm{H}(X)$ (resp. $\mathrm{h}(X)$).

2. FRAMEWORK AND MULTILEVEL CODING

Within the scope of this paper, the print-and-scan channel is studied only for the case of B&W halftone printers and low-resolution CCD-based scanners (up to 600 ppi). However, our approach can be easily extended and applied to other type of devices. In this section, we derive an upper bound on the maximum achievable rate of reliable communications over this particular instance of the print-and-scan channel. We also review the fundamentals of multilevel coding for the AWGN channel.

2.1. Upper bound on the maximum achievable rate

Halftone printers simulate multiple gray levels by using the so-called halftoning[3] technique. It is fairly easy to compute an upper bound on the maximum achievable rate of 2D bar codes when a halftone printer implementing clustered-dot ordered dithering[3] is used (e.g. laser printer). For this purpose, assume that ideal printer and scanner devices are exploited so that the ISI can be avoided. Furthermore, suppose perfect synchronization, meaning that all 2D symbols can be perfectly read. Let r_p represent the printer's resolution measured in dots per inch (dpi), a be the length in dots of the side of a square halftone cell* (Figure 1(a)), and r_s denote the scanner's resolution measured in pixels per inch (ppi). In this case, the printer produces $(r_p/a)^2$ halftone cells

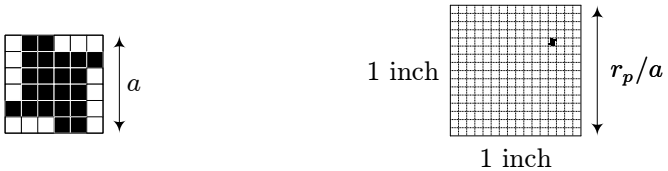

Figure 1. Clustered-dot ordered dithering. (a) Square halftone cell of a-by-a dots. (b) Array of halftone cells.

per square inch (Figure 1(b)) and each halftone cell can represent up to a^2+1 equivalent gray levels.[3] Assuming we use a halftone cell as 2D symbol, we can place up to:

$$U = (r_p/a)^2 \cdot \log_2(a^2+1) \tag{1}$$

information bits per square inch. This upper bound is strictly decreasing for positive integer values of a (Figure 2). At first, since the maximum value is obtained for $a = 1$, it seems that the best one can do is to use only B&W symbols. However, for this situation, the minimum scanner resolution to be used is $r_s \geq r_p$, which is incongruent to our low-resolution requirement for this device. On the other hand, if $a > 1$, meaning that we use $a^2 + 1$ gray

*The quotient r_p/a (Figure 1(b)) is usually known as the printer's screen frequency and is measured in lines per inch (lpi).

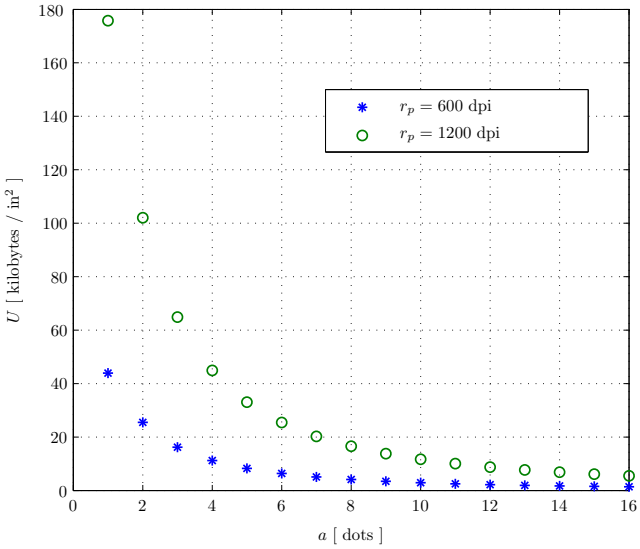

Figure 2. Upper bound on the maximum achievable rate of multilevel 2D bar codes when a halftone printer implementing clustered-dot ordered dithering is used.

levels, the minimum scanner resolution to be used is $r_s \geq r_p/a$. This implies that for given printer and scanner resolutions there is an optimum number of gray levels to be used, which is $(r_p/r_s)^2 + 1$ for our ideal setup, such that the achievable rate of the multilevel 2D bar code is maximized.

2.2. Multilevel coding for the AWGN channel

The idea of coded modulation is to jointly optimize coding and modulation in order to improve the performance of digital communication schemes.[4] Multilevel coding with multistage decoding, multilevel coding with parallel independent decoding, and bit-interleaved coded modulation are three well-known bandwidth-efficient schemes for the AWGN channel in the high-SNR regime.[5–11] In the following paragraphs we recall the fundamental ideas behind these coded modulation schemes.

Consider the discrete-time AWGN channel:

$$Y = X + Z, \qquad X \in \mathcal{X}, \qquad Y \in \mathcal{Y}, \qquad Z \sim \mathcal{N}(0, \sigma_Z^2), \tag{2}$$

where $\mathcal{X}$ (resp. $\mathcal{Y}$) is the input (resp. output) alphabet, X (resp. Y) is the channel input (resp. output) and Z represents the noise. For each channel use, the noise Z is drawn i.i.d. from a zero-mean Gaussian distribution with variance σ_Z^2 and is assumed to be independent from the channel input X. Given the channel input variance σ_X^2, the capacity of this channel, in bits per channel use, is:

$$C_{\text{AWGN}} = \max_{p_X(\cdot)} \mathrm{I}(X;Y) = \frac{1}{2}\log_2\left(1 + \frac{\sigma_X^2}{\sigma_Z^2}\right), \tag{3}$$

which is attained when the channel input X is Gaussian, say $X \sim \mathcal{N}(0, \sigma_X^2)$.

Due to the technical impossibility of using either a continuous or an infinite input alphabet, practical systems usually employ a discrete and finite $M = 2^L-$ary input alphabet (signal constellation), i.e. $|\mathcal{X}| = 2^L$. It is then customary to assign a label (binary address vector) to each signal point by means of a bijective mapping μ:

$$(x^0, x^1, \ldots, x^{L-1}) \underset{\mu}{\mapsto} x, \qquad x^i \in \mathcal{B} = \{0,1\}, \qquad x \in \mathcal{X}, \qquad i = 0, 1, \ldots, L-1. \tag{4}$$

Given a specific probability distribution $\{p(x) : x \in \mathcal{X}\}$ over the channel inputs, the maximum rate of reliable communications of such systems is given by the mutual information $\mathrm{I}(X;Y)$ between the channel input X and

the channel output Y. We now briefly review MLC/MSD, MLC/PID, and BICM, which are coded modulation schemes capable of approaching $\mathrm{I}(X;Y)$[†]. The reader is encouraged to consult the corresponding references for more details.

Remarkably, MLC/MSD[6–8] is a straightforward consequence of the chain rule for mutual information. Since the mapping μ in (4) is bijective, the mutual information $\mathrm{I}(X;Y)$ between the transmitted signal X and the received signal Y equals the mutual information $\mathrm{I}(X^0, X^1, \ldots, X^{L-1}; Y)$ between the address vector and the received signal Y. Applying the chain rule for mutual information, we get:

$$\begin{aligned}\mathrm{I}(X;Y) &= \mathrm{I}(X^0, X^1, \ldots, X^{L-1}; Y) \\ &= \mathrm{I}(X^0;Y) + \mathrm{I}(X^1;Y|X^0) + \ldots + \mathrm{I}(X^{L-1};Y|X^0, X^1, \ldots, X^{L-2}).\end{aligned} \tag{5}$$

Equation (5) may be interpreted as follows. Transmission of vectors with binary digits $x^i, i = 0, 1, \ldots, L-1$, over the physical channel can be separated into the parallel transmission of individual bits x^i over L equivalent channels, provided that $x^0, x^1, \ldots, x^{i-1}$ are known. At the transmitter side (Figure 3), a binary data block of length K bits is partitioned into L sub-blocks:

$$\mathbf{q} = (q_1, \ldots, q_K), \qquad q_k \in \mathcal{B}, \qquad k = 1, \ldots, K, \tag{6}$$

$$\mathbf{q} = (\mathbf{q}^0, \ldots, \mathbf{q}^{L-1}), \qquad \mathbf{q}^i = (q_1^i, \ldots, q_{K_i}^i), \qquad i = 0, 1, \ldots, L-1, \qquad \sum_{i=0}^{L-1} K_i = K. \tag{7}$$

Each data sub-block $\mathbf{q}^i$ is fed into an individual binary encoder E_i of rate $R_i = K_i/N$ producing a codeword:

$$\mathbf{x}^i = (x_1^i, \ldots, x_N^i), \qquad x_n^i \in \mathcal{B}, \qquad n = 1, \ldots, N, \qquad i = 0, 1, \ldots, L-1, \tag{8}$$

of the corresponding component code. In this manner L levels of coding are created. In principle, any binary

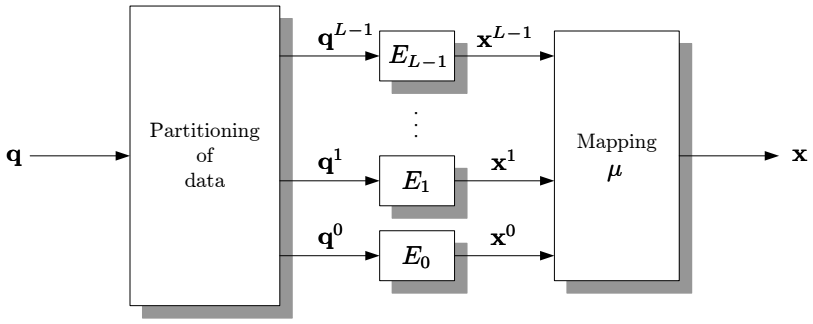

Figure 3. Multilevel encoder.

code can be used as a component code, e.g. block codes, convolutional codes, concatenated codes, etc.[12–14] For simplicity, we assume that all codewords have equal length, N bits, at all levels. Then, the n-th bit x_n^i, $n = 1, \ldots, N$, of every codeword $\mathbf{x}^i$ is selected to form a binary label $(x_n^0, x_n^1, \ldots, x_n^{L-1})$ of L bits, which is mapped via μ to a signal point $x_n \in \mathcal{X}$. In this way, we obtain a vector:

$$\mathbf{x} = (x_1, \ldots, x_N), \qquad x_n \in \mathcal{X}, \qquad n = 1, \ldots, N, \tag{9}$$

of N channel inputs, which are serially transmitted over the AWGN channel. It is very easy to show that the code rate of the overall scheme, $R = K/N$, is equal to the sum of the individual code rates, i.e.:

$$\sum_{i=0}^{L-1} R_i = \sum_{i=0}^{L-1} \frac{K_i}{N} = \frac{1}{N} \sum_{i=0}^{L-1} K_i = \frac{K}{N} = R. \tag{10}$$

[†]In order to approach the capacity of the AWGN channel, i.e. $\max_{p_X(\cdot)} \mathrm{I}(X;Y)$, these schemes need to combine coding with signal shaping.

At the receiver side, the component codes are successively decoded by the corresponding decoders starting from the lowest level. At any stage i, $i = 0, 1, \ldots, L-1$, the decoder processes not only the N received signal points:

$$\mathbf{y} = (y_1, \ldots, y_N), \qquad y_n \in \mathcal{Y}, \qquad n = 1, \ldots, N, \tag{11}$$

but also decisions of previous decoding stages:

$$\hat{\mathbf{x}}^j = (\hat{x}_1^j, \ldots, \hat{x}_N^j), \qquad \hat{x}_n^j \in \mathcal{B}, \qquad n = 1, \ldots, N, \qquad j = 0, 1, \ldots, i-1. \tag{12}$$

The block diagram of the receiver is shown in Figure 4. For simplicity, this diagram doest not represent neither the 'Data selection' block, which outputs $\hat{\mathbf{q}}^0, \ldots, \hat{\mathbf{q}}^{L-1}$ nor the 'Concatenation of data' block, which outputs $\hat{\mathbf{q}}$. One can demonstrate that MLC/MSD corresponds to transmission over L equivalent channels and prove

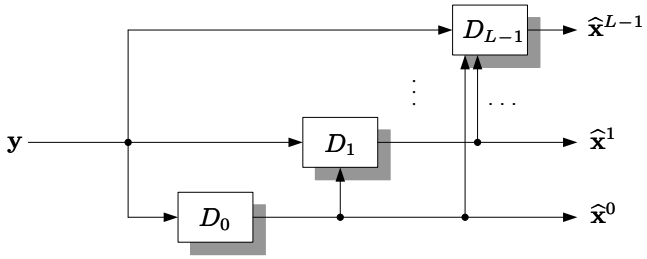

Figure 4. Multistage decoder.

that the maximum achievable rate of a modulation scheme (e.g. 8–PAM) with given a-priori probabilities of its signal constellation points can indeed be achieved by MLC/MSD if, and only if, the individual rates R_i of the component codes are chosen to be equal to the capacities of the equivalent channels, i.e:

$$R_i = \mathrm{I}(X^i; Y | X^0, X^1, \ldots, X^{i-1}), \qquad i = 0, 1, \ldots, L-1. \tag{13}$$

This is the so-called *capacity rule* for choosing the individual code rates.[7] In principle, there is no restriction on the particular labeling used in MLC/MSD. Nevertheless, for finite codeword length, Ungerböck's labeling turns out to lead to the highest performance among MLC/MSD schemes with different labelings.

In the MLC/PID[7, 8] approach, the decoders do not process decisions of previous levels, meaning that individual levels are decoded in parallel (Figure 5). In contrast to the MLC/MSD scheme, the maximum achievable

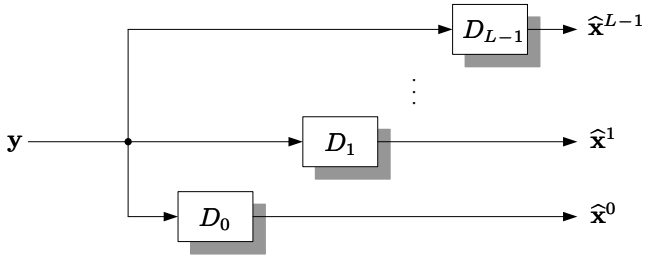

Figure 5. Parallel independent decoder.

rate of a modulation scheme using MLC/PID strongly depends on the particular labeling of signal points. Nevertheless, it can be shown that for very large codeword lengths N, the performance gap between MLC/PID and MLC/MSD is very small when Gray labeling is used.[7] Similar results with respect to how to choose the individual rates of the component codes can also be obtained for this scheme.

BICM[9, 10] was first proposed for fading channels, but turned out to be capable of approaching the capacity of the AWGN channel in the high-SNR regime. Moreover, it can be shown that BICM is actually a derivative

of the MLC/PID scheme using a single binary code. A BICM transmitter comprises an encoder for a binary code C, a bit interleaver, and a signal mapper. The output sequence of the bit interleaver is segmented into L-bit blocks, which are mapped into a signal point of a 2^L-ary constellation using Gray labeling. A BICM transmitter and receiver pair is shown in Figure 6. Although BICM cannot operate arbitrarily close to capacity,

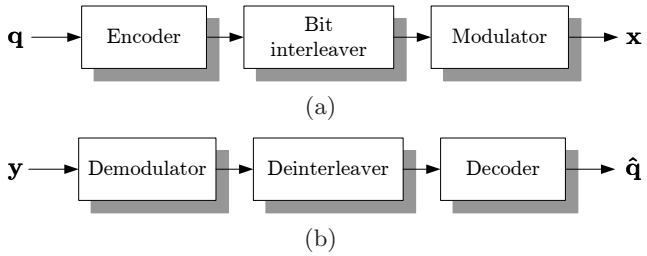

Figure 6. Bit interleaved coded modulation. (a) BICM transmitter. (b) BICM receiver.

good performance close to capacity can be obtained if C is a long parallel or serially concatenated Turbo code, and the decoder is an iterative Turbo decoder.[9]

3. PRINT-AND-SCAN CHANNEL MODEL

We consider the problem of data transmission via the print-and-scan channel as a digital communications problem in the high-SNR regime. Thus a 2D bar code symbol is modeled as a signal (pulse) and signaling using multiple gray levels is modeled by pulse amplitude modulation (PAM).

The print-and-scan channel is such that it introduces several types of distortions, specifically, luminance transformations, scaling, rotation, low pass filtering, aliasing, and noise. Furthermore, its behavior will depend on the selected image resolution (in ppi); the parameters used for printing, namely, resolution (in dpi), screen frequency (in lpi), and halftoning algorithm; and the parameters used for scanning, namely, resolution (in ppi), bit-depth, tone correction (e.g. γ-correction), and driver filters (e.g. descreening filter).

Let r_i be the selected image resolution. Without loss of generality, we only consider the case in which $r_s \geq r_i$. Although a general model of the print-and-scan channel has been proposed for the case when $r_s = r_i$,[15,16] we do not use it here because, in general, a synchronization algorithm is required in this case for correctly reading and decoding the 2D symbols. Since in this work we do not address synchronization problems, we only consider the case in which $r_s > r_i$ and make some assumptions in order to simplify the channel model.

Let us fix the shape of the 2D symbol to be a square and use some space between symbols to avoid the ISI produced by the print-and-scan channel.[16] In Figure 7, we show an example of such a multilevel 2D bar code.

Figure 7. Eight–level 2D bar code. (a) Original digital image: 2×2 pixel symbols, 1 pixel of inter-symbol space, $r_i = 200$ ppi. (b) Printed-and-scanned digital image: $r_p = 600$ dpi, $r_s = 3 \cdot r_i = 600$ ppi, 6×6 pixel noisy symbols.

Based on our experimental results, reported in Sections 5.1 and 5.2, we model the print-and-scan channel as:

$$Y = \varphi(X) + Z, \qquad X \in \mathcal{X}, \qquad Y \in \mathcal{Y} = \mathbb{R}, \tag{14}$$

where X (the channel input) represents the gray value of a 2D symbol, $\varphi : \mathcal{X} \to [-1, +1]$ is a nonlinear function representing the response of the print-and-scan channel, Z represents zero-mean additive noise, and Y (the channel output) represents the obtained gray value of the corresponding 2D symbol. Gray values are represented as numbers in the interval $[-1, +1]$[‡]. For an M–ary multilevel 2D bar code system, we have $|\mathcal{X}| = M$. The function $\varphi(\cdot)$ is in general different for every particular instance of the print-and-scan channel, i.e. for every printer and scanner combination. Contrary to what is usually assumed, the noise term Z is not assumed to be independent of the gray value X. In fact, we approximate the probability distribution of Z by a Gaussian distribution with variance depending on the channel input X. Thus, we model Z as:

$$Z = \sigma_Z(X) \cdot W, \tag{15}$$

where, for each channel use, W is drawn i.i.d. from a standard normal distribution $\mathcal{N}(0, 1)$ independently from X, and $\sigma_Z : \mathcal{X} \to \mathbb{R}^+$ is a function that determines the noise variance given the channel input X.

Our print-and-scan channel model is depicted in Figure 8. This figure does not explicitly show the modulation

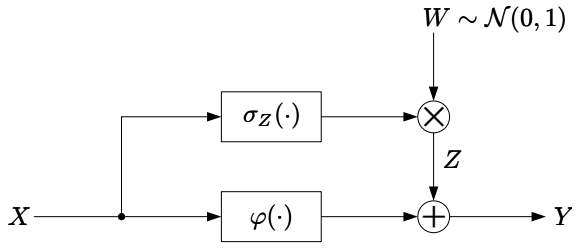

Figure 8. Model for the print-and-scan channel.

and demodulation steps. Given a gray value X, the modulation step consists in creating a square (e.g. a 2×2 pixel square) with gray value X and the demodulation step consists in determining the gray value Y best describing the received square (e.g. a 4×4 pixel square if $r_s = 2 \cdot r_i$). Notice also that our channel model assumes perfect synchronization at the receiver side. A block diagram showing the different elements considered in our model is depicted in Figure 9. Observe that since the demodulation algorithm is to be chosen, the performance of a multilevel 2D bar code system will be influenced by the demodulation step.

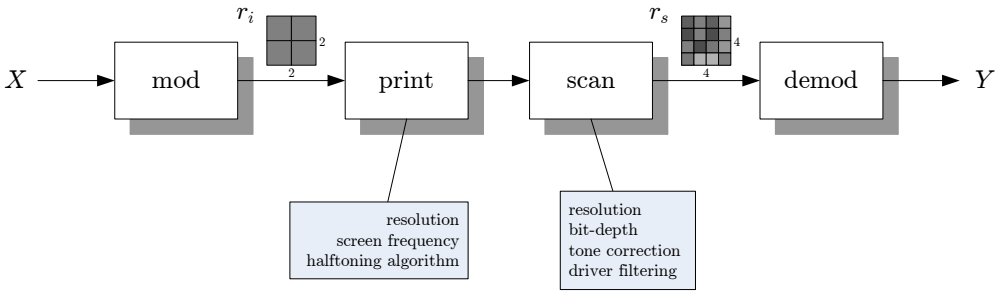

Figure 9. Modulation and demodulation steps for communications over the print-and-scan channel.

As a final remark, notice that we can guarantee that our system works in the high-SNR regime by making the 2D symbols large enough (or equivalently, increasing their energy). This condition being satisfied allows us to use powerful coded modulation techniques.

[‡]It is customary to encode 8-bit gray images using decimal numbers from 0 (black) to 255 (white). We use the linear transform $T(x) = \frac{2}{255}x - 1$ in order to normalize gray values to the interval $[-1, +1]$.

4. MULTILEVEL CODING FOR PRINT-AND-SCAN CHANNELS

In this section, we extend the theory of MLC/MSD to the case of the print-and-scan channel modeled by (14) and (15).

Suppose we use an M–ary ($|\mathcal{X}| = M = 2^L$) modulation system with given a-priori probabilities of the signal constellation points $\{p(x) : x \in \mathcal{X}\}$. Since our channel is memoryless, i.e. the output Y depends solely on the current channel input X and current noise term Z, the maximum rate of reliable communications is given by the mutual information $\mathrm{I}(X;Y)$. Although we cannot provide a closed-form expression for $\mathrm{I}(X;Y)$ it is fairly easy to compute it numerically. By definition:

$$\mathrm{I}(X;Y) = \mathrm{h}(Y) - \mathrm{h}(Y|X). \tag{16}$$

Firstly, we can compute the term $\mathrm{h}(Y)$ in (16) as follows. By definition:

$$\mathrm{h}(Y) = -\int_{\mathcal{Y}} f(y) \log f(y) \, \mathrm{d}y. \tag{17}$$

In order to numerically compute the integral in (17), we need to specify $f(y)$. This can be done by conditioning on X:

$$f(y) = \sum_{x \in \mathcal{X}} f(y|x)p(x). \tag{18}$$

The term $f(y|x)$ in (18) can be obtained noting that $Y|X = x$ has a Gaussian distribution with mean $\varphi(x)$ and variance $\sigma_Z^2(x)$, i.e. $(Y|X = x) \sim \mathcal{N}(\varphi(x), \sigma_Z^2(x))$.

Secondly, the term $\mathrm{h}(Y|X)$ in (16) can be computed as follows:

$$\mathrm{h}(Y|X) = \mathrm{h}(\varphi(X) + Z|X) = \mathrm{h}(Z|X) = \sum_{x \in \mathcal{X}} \mathrm{h}(Z|X = x)p(x), \tag{19}$$

where we used (14) and the definition of conditional differential entropy. Since $Z|X = x$ has a Gaussian distribution with zero mean and variance $\sigma_Z^2(x)$, we have $\mathrm{h}(Z|X = x) = \frac{1}{2}\log(2\pi e\sigma_Z^2(x))$. Therefore,

$$\mathrm{h}(Y|X) = \sum_{x \in \mathcal{X}} \frac{1}{2}\log(2\pi e\sigma_Z^2(x))p(x) = \mathrm{E}_{p_X}\left[\frac{1}{2}\log(2\pi e\sigma_Z^2(X))\right]. \tag{20}$$

Although we are able to compute $\mathrm{I}(X;Y)$ for any given input distribution $p_X(\cdot)$, the problem of finding the capacity $\max\limits_{p_X(\cdot)} \mathrm{I}(X;Y)$ of the print-and-scan channel is more involved. The difficulty arises from the fact that both terms in the right-hand-side of (16) depend on $p_X(\cdot)$.

However, we can follow the same reasoning and notation as in Section 2.2 and still make use of MLC/MSD in order to approach $\mathrm{I}(X;Y)$. The main difference with respect to the AWGN channel is that in our case we have to take into account the dependence of the channel input X and the noise Z. For $i = 0, 1, \ldots, L-1$, the individual rates R_i of the component codes can be computed as follows:

$$R_i = \mathrm{I}(X^i; Y|X^0, \ldots, X^{i-1}) = \mathrm{h}(Y|X^0, \ldots, X^{i-1}) - \mathrm{h}(Y|X^0, \ldots, X^{i-1}, X^i). \tag{21}$$

We compute the term $\mathrm{h}(Y|X^0, \ldots, X^{i-1})$ in (21) as follows. By definition:

$$\mathrm{h}(Y|X^0, \ldots, X^{i-1}) = \sum_{(x^0,\ldots,x^{i-1}) \in \mathcal{B}^i} \mathrm{h}(Y|X^0 = x^0, \ldots, X^{i-1} = x^{i-1})p(x^0, \ldots, x^{i-1}), \tag{22}$$

and

$$\mathrm{h}(Y|X^0 = x^0, \ldots, X^{i-1} = x^{i-1}) = -\int_{\mathcal{Y}} f(y|x^0, \ldots, x^{i-1}) \log f(y|x^0, \ldots, x^{i-1}) \, \mathrm{d}y. \tag{23}$$

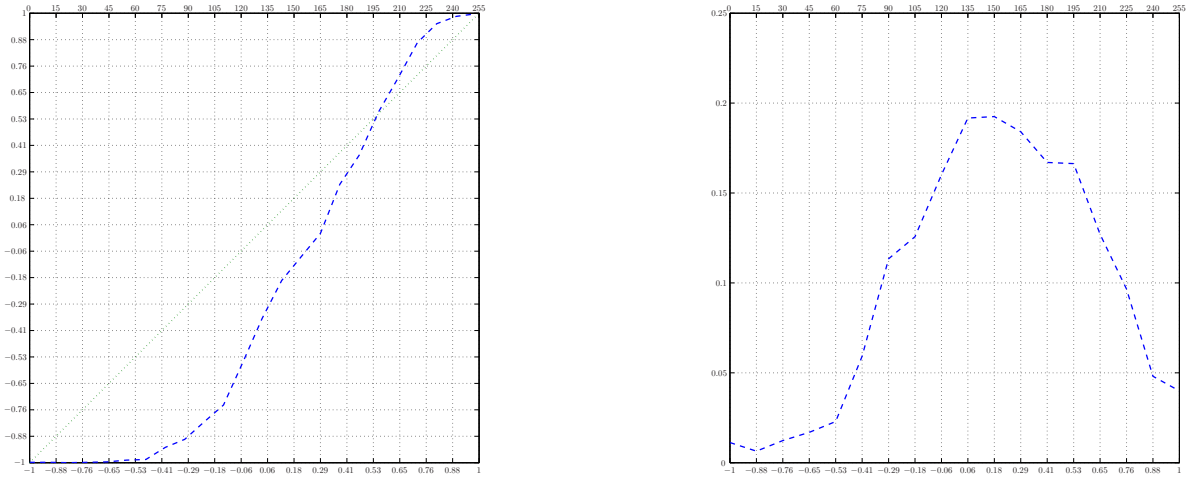

(a) (b)

Figure 10. Print-and-scan channel characterization. (a) Sample mean $\hat{\mu}_{Y|X}(x)$. (b) Square root of the sample variance $\hat{\sigma}^2_{Y|X}(x)$.

Hence, in order to compute $\mathrm{h}(Y|X^0 = x^0, \ldots, X^{i-1} = x^{i-1})$ we need to specify $f(y|x^0, \ldots, x^{i-1})$. This can be done by conditioning on $X^i, \ldots, X^{L-1}$:

$$\begin{aligned} f(y|x^0, \ldots, x^{i-1}) &= \sum_{(x^i, \ldots, x^{L-1}) \in \mathcal{B}^{L-i}} f(y|x^0, \ldots, x^{i-1}, x^i, \ldots, x^{L-1}) p(x^i, \ldots, x^{L-1}) \\ &= \sum_{(x^i, \ldots, x^{L-1}) \in \mathcal{B}^{L-i}} f(y|\mu(x^0, \ldots, x^{L-1})) p(x^i, \ldots, x^{L-1}). \end{aligned} \tag{24}$$

Exactly like for $f(y)$ in (18), $f(y|\mu(x^0, \ldots, x^{L-1}))$ can be obtained noting that $(Y|X = x) \sim \mathcal{N}(\varphi(x), \sigma^2_Z(x))$.

Obviously, we can proceed in the same manner in order to compute the term $\mathrm{h}(Y|X^0, \ldots, X^{i-1}, X^i)$ in (21). Finally, notice that since $f(y|\mu(x^0, \ldots, x^{L-1}))$ depends on the actual mapping μ, R_i in (21) will also be mapping dependent for $i = 0, 1, \ldots, L-1$.

5. COMPUTER SIMULATION RESULTS

The experimental study performed in the scope of this work can be divided in three parts: characterization of the print-and-scan channel, rate design for MLC/MSD over the print-and-scan channel, and performance results of MLC/MSD in terms of achievable rate and bit error rate (BER). We exploited the following equipment in our experiments:

- Halftone printer: HP Color LaserJet 4600 (B&W mode, 600 dpi);
- CCD-based scanner: Epson Perfection 3170 Photo.

The settings that were used for the experiments are described below. Printer: resolution $r_p = 600$ dpi, default screen frequency, and default halftoning algorithm. Scanner: $r_s = 600$ ppi, 8 bits of bit-depth, black point set to 23, white point set to 248, γ–correction set to 1, and no driver filtering.

Furthermore, we used 2×2 pixel 2D symbols and 1 pixel of inter-symbol space. The image resolution parameter r_i of all our digital images was set to 200 ppi. Finally, the demodulation algorithm (Figure 9) we used consisted in averaging the gray values of all but the borderline pixels of a noisy 2D symbol[§]. As an example,

[§]We do not take into account borderline pixels in order to reduce desynchronization problems. The choice $r_s = 3 \cdot r_i$ is justified by the same reason.

we show in Figure 7 the original and noisy versions of a 2D multilevel bar code printed-and-scanned under the above conditions.

5.1. Characterization of the print-and-scan channel

In this experiment, all gray levels from 0 (black) to 255 (white) were used. For each gray level $x \in [-1, +1]$, $J = 200$ bar code symbols with gray level x were sent through the print-and-scan channel. Then, the sample mean $\hat{\mu}_{Y|X}(x)$ and sample variance $\hat{\sigma}^2_{Y|X}(x)$ of the received noisy symbols $y_j(x) \in \mathbb{R}$, $j = 1, \ldots, J$, were computed[¶]. We show in Figures 10(a) and 10(b) the obtained results for all the 256 tested gray levels.

The channel response $\varphi(\cdot)$ was then approximated by the sample mean $\hat{\mu}_{Y|X}(x)$, i.e. $\varphi(x) = \hat{\mu}_{Y|X}(x)$, and the noise variance $\sigma^2_Z(\cdot)$ by the sample variance $\hat{\sigma}^2_{Y|X}(x)$, i.e. $\sigma^2_Z(x) = \hat{\sigma}^2_{Y|X}(x)$.

5.2. Rate design for MLC/MSD over the print-and-scan channel

First, by using the estimated $\varphi(\cdot)$ and $\sigma^2_Z(\cdot)$, we selected a signal constellation $\mathcal{X}$ in such a way that the *received* signal points were close to each other where the noise variance was small and farther apart where the noise variance was large. Specifically, we selected the following non-equidistant 8–PAM signal constellation:

$$\mathcal{X} = \{0, 99, 120, 141, 176, 199, 216, 255\}. \tag{25}$$

In Figure 11, we schematize the employed algorithm for selecting this constellation.

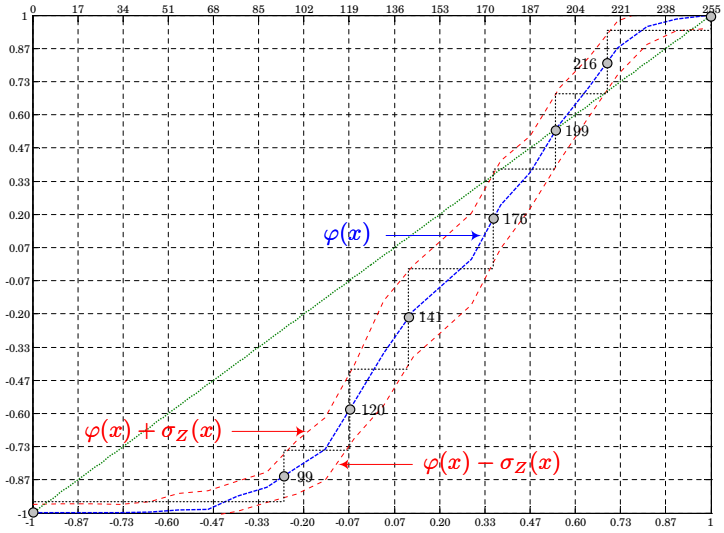

Figure 11. Non-equidistant 8–PAM signal constellation.

Second, we assigned uniform priors to the signal points in $\mathcal{X}$ and sent each of them 3200 times over the print-and-scan channel. We show in Figure 12 the frequency distribution of the received signal points for each $x \in \mathcal{X}$. We observe from this figure that given a signal point $x \in \mathcal{X}$, the conditional noise distribution $f_{Z|X}(\cdot|x)$ can be approximated, at first order, by a Gaussian distribution with mean $\varphi(x)$ and variance $\sigma^2_Z(x)$.

Finally, by using the procedure described in Section 4, we numerically computed the rates R_i, $i = 0, 1, 2$, of a non-equidistant 8–PAM MLC/MSD scheme employing Ungerböck's labeling:

$$R_0 = 0.519, \qquad R_1 = 0.981, \qquad R_2 = 1. \tag{26}$$

[¶]The following estimators were used: $\hat{\mu}_{Y|X}(x) = \frac{1}{J}\sum_{j=1}^{J} y_j(x)$ and $\hat{\sigma}^2_{Y|X}(x) = \frac{1}{J-1}\sum_{j=1}^{J}(y_j(x) - \hat{\mu}_{Y|X}(x))^2$.

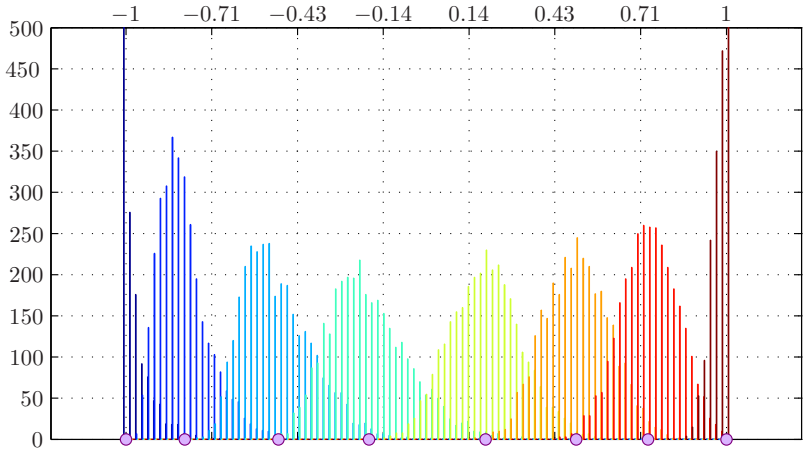

Figure 12. Frequency distribution of the received signal points for each $x \in \mathcal{X}$.

5.3. Performance results of MLC/MSD over the print-and-scan channel

We implemented a non-equidistant 8–PAM MLC/MSD scheme using the parameters obtained in Sections 5.1 and 5.2. For the component codes of individual levels we used low-density parity-check (LDPC) codes. Specifically, we used the Matlab implementation of quasi-regular LDPC codes from I. Kozintsev.[17]

The multilevel encoder has a straightforward implementation. For the multistage decoder, one should take into account the derived print-and-scan channel statistics in order to correctly compute the log-likelihood ratios used in the LDPC belief propagation algorithm:

$$l_n^i = \ln \frac{f_{Y|X^i,X^0,\ldots,X^{i-1}}(y_n|1,\hat{x}^0,\ldots,\hat{x}^{i-1})}{f_{Y|X^i,X^0,\ldots,X^{i-1}}(y_n|0,\hat{x}^0,\ldots,\hat{x}^{i-1})}, \qquad i=0,\ldots,L-1, \qquad n=1,\ldots,N. \tag{27}$$

For a block length of $N = 2048$ bits, the rate of our scheme was 1403 bytes/in^2 at a bit error rate (BER) of 2×10^{-4}. For comparison, the rate of the uncoded version of our multilevel 2D bar code is 1684 bytes/in^2 at a BER of 4×10^{-2} and the rate of DataMatrix,[18] a commercial high-rate B&W 2D bar code, is 375 bytes/in^2. Although, the current BER might not be small enough, we are persuaded that by using *irregular* LDPC codes and larger block lengths, we are able to reduce the BER to an acceptable level.

6. CONCLUSION AND FUTURE WORK

In this work, we highlighted the attractiveness of multilevel 2D bar codes for high capacity storage applications. We have also shown how to apply powerful coded modulation schemes developed for the AWGN channel to the print-and-scan channel in the context of multilevel 2D bar codes. Key point is the construction of a simplified model of the print-and-scan channel specifically adapted for this application. Our approach can be applied to other printing and reading devices as well as to enhance existing B&W 2D bar codes. Finally, the experimental results show that, under the same conditions, optimally designed multilevel 2D bar codes can reliably achieve higher rates than their B&W counterparts and can therefore meet the high capacity storage requirements of many new multimedia security and data management applications.

In future work, we plan to investigate the synchronization problem of print-and-scan channels in the context of multilevel 2D bar codes.[16] A good synchronization algorithm would lead to a reduction in BER and the possibility to use lower scanner resolutions, e.g. $r_s = 2 \cdot r_i$. Moreover, since our practical system neglects the border of the received 2D symbols when performing the demodulation step, a significant improvement in terms of achievable rate may be obtained by eliminating the inter-symbol space. Finally, a more general framework where the ISI is fully considered is to be investigated.

ACKNOWLEDGMENTS

This paper was partially supported by the Swiss National Science Foundation (SNF) professorship grant No. PP002-68653/1, the Interactive Multimodal Information Management (IM2) project and by the European Commission through the IST programme under contract IST-2002-507932 ECRYPT. The authors are thankful to the members of the Stochastic Image Processing group at the University of Geneva for many helpful and interesting discussions. R. Villán wishes to thank R. Urbanke for assisting in the understanding of coded modulation schemes, and A. Villalba for performing some of the experimental work. The information in this document reflects only the author's views, is provided as is and no guarantee or warranty is given that the information is fit for any particular purpose. The user thereof uses the information at its sole risk and liability.

REFERENCES

1. D. Kirovski, N. Jojic, and G. Jancke, "Tamper-Resistant Biometric IDs," in *Information Security Solutions Europe*, (Berlin, Germany), September 28-30 2004.
2. S. Voloshynovskiy, O. Koval, F. Deguillaume, and T. Pun, "Visual communications with side information via distributed printing channels: extended multimedia and security perspectives," in *Proceedings of SPIE Photonics West, Electronic Imaging 2004, Multimedia Processing and Applications*, (San Jose, USA), January 18-22 2004.
3. D. L. Lau and G. R. Arce, *Modern Digital Halftoning*, Marcel Dekker, Inc., New York - Basel, 2001.
4. J. L. Massey, "Coding and Modulation in Digital Communications," in *Proceedings of Intern. Zürich Seminar on Digital Communications*, pp. E2(1)–E2(4), 1974.
5. G. Forney and G. Ungerboeck, "Modulation and Coding for Linear Gaussian Channels," *IEEE Transactions on Information Theory* **44**, pp. 2384–2415, October 1998.
6. H. Imai and S. Hirakawa, "A New Multilevel Coding Method Using Error-Correcting Codes," *IEEE Transactions on Information Theory* **23**, pp. 371–377, May 1977.
7. U. Wachsmann, R. F. H. Fischer, and J. B. Huber, "Multilevel Codes: Theoretical Concepts and Practical Design Rules," *IEEE Transactions on Information Theory* **45**, pp. 1361–1391, July 1999.
8. U. Wachsmann, *Coded Modulation: Theoretical Concepts and Practical Design Rules*. Ph.D. dissertation, Technischen Fakultät der Universität Erlangen-Nürnberg, July 1999.
9. G. Caire, G. Taricco, and E. Biglieri, "Bit-Interleaved Coded Modulation," *IEEE Transactions on Information Theory* **44**, pp. 927–946, May 1998.
10. G. Caire, G. Taricco, and E. Biglieri, "Capacity of bit-interleaved channels," *Electronic Letters* **32**, pp. 1060–1061, June 1996.
11. J. Hou, P. H. Siegel, L. B. Milstein, and H. D. Pfister, "Capacity-Approaching Bandwidth-Efficient Coded Modulation Schemes Based on Low-Density Parity-Check Codes," *IEEE Transactions on Information Theory* **49**, pp. 2141–2155, September 2003.
12. R. E. Blahut, *Theory and Practice of Error Control Codes*, Addison-Wesley Publishing Company, 1989.
13. C. Berrou, A. Glavieux, and P. Thitimajshima, "Near Shannon limit error-correcting coding and decoding: Turbo-Codes," in *IEEE Int. Conf. on Communications*, **2**, pp. 1064–1070, (Geneva, Switzerland), May 1993.
14. S. Chung, J. G. D. Forney, T. Richardson, and R. Urbanke, "On the design of low-density parity-check codes within 0.0045 db of the shannon limit," *IEEE Communications Letters* **5**, pp. 58–60, Feb. 2001.
15. A. K. Jain, *Fundamentals of Digital Image Processing*, Prentice-Hall International, Inc., 1989.
16. N. Degara-Quintela and F. Perez-Gonzalez, "Visible Encryption: Using Paper as a Secure Channel," in *Electronic Imaging: Security and Watermarking of Multimedia Contents V*, E. J. D. III and P. W. Wong, eds., *Proc. SPIE* **5020**, pp. 413–422, 2003.
17. I. Kozintsev, "Matlab programs for encoding and decoding of LDPC codes over GF(2^m) (600 KB)." `http://www.kozintsev.net/soft.html`. Available by November 30th, 2004.
18. IDAutomation.com, "Data Matrix Barcode FAQ & Tutorial." `http://idautomation.com/datamatrixfaq.html`. Available by November 30th, 2004.